Available online at www.sciencedirect.com

jmr&t Journal of Materials Research and Technology

www.jmrt.com.br

Original Article

Fabrication of calcium phosphate coating on pure magnesium substrate via simple chemical conversion coating: surface properties and corrosion performance evaluations

Mohd Amin Farhan Zaludin[a,b,*], *Zul Azhar Zahid Jamal*[a,c], *Mohd Nazree Derman*[a,b], *Mohd Zaheruddin Kasmuin*[a,b]

[a] *Centre of Excellence (COE) Frontier Materials Research. School of Materials Engineering, Universiti Malaysia Perlis (UniMAP), Blok B, Taman Pertiwi Indah, 01000 Kangar, Perlis, Malaysia*

[b] *School of Materials Engineering, Universiti Malaysia Perlis (UniMAP), Taman Muhibbah, Jejawi, 02600 Arau, Perlis, Malaysia*

[c] *School of Microelectronic Engineering, Universiti Malaysia Perlis (UniMAP), Pauh Putra Campus, 02600 Arau, Perlis, Malaysia*

ARTICLE INFO

Article history:
Received 29 January 2018
Accepted 25 June 2018
Available online 20 August 2018

Keywords:
Magnesium
Calcium phosphate coating
Chemical conversion coating

ABSTRACT

The main objective of the current work was to fabricate calcium phosphate (CaP) coating on 99.9% purity magnesium, Mg substrate through simple chemical conversion method and evaluated the surface properties and corrosion performance of the coated substrates. The chemical conversion method was done by immersing the samples inside primary phosphating bath and followed by secondary treatment in alkaline solutions. The coated samples from the primary (PRI) and secondary (SEC) coating treatment were analyzed from morphological, topographical, and phase analysis aspects. The corrosion behaviour of the coatings inside simulated body fluid was assessed by potentiodynamic polarization (PDP) and electrochemical impedance spectroscopy (EIS). The PRI and SEC coated were composed of dicalcium phosphate dehydrate (DCPD) and hydroxyapatite (HA), respectively. Both of the coatings improved the corrosion resistance of the Mg substrate. The corrosion potentials, E_{corr} of the coated samples becomes nobler compared to the bare substrates. EIS shows that the polarization resistance, R_p is improved about 40 and 2 times fold for PRI and SEC compared to the uncoated samples. Furthermore, PRI shows better corrosion resistance compared to SEC due to lower porosity along with thicker and better coating coverage.

* *Corresponding author.*
E-mail: aminzaludin90@yahoo.com (M.A.F. Zaludin).

https://doi.org/10.1016/j.jmrt.2018.06.017

1. Introduction

Metallic implants are more favoured for orthopaedic applications such as immobilization and bone fracture fixation device due to their excellent mechanical properties compared to polymers and ceramic materials [1]. Mg alloys have gained popularity as revolutionary implant materials that applied to handle the bioinert problem with the current conventional implant materials. Mg are well known for its biodegradability, matched mechanical properties with natural bones, and especially biocompatibility with the physiological environment [2,3]. Biodegradable properties of the Mg is governed by its high reactivity and corrosion process inside aqueous solutions [2,4]. However, the corrosion rate of the Mg is higher compared to sufficient healing periods. Thus, there is a necessity to control the fast degradation rate of Mg, so that the Mg based implants could maintain the mechanical integrity, hence keep functioning as supports or orthopaedic devices and safely excreted from the human body via urine disposal [2]. Several strategies have been employed to improve the corrosion resistance of Mg such as selection of alloying element [5–8] and development of composite reinforced with bioactive ceramic phase [9,10]. Even though these strategies are working in order to reduce the corrosion rate of Mg, it seems that the corrosion rate is still high.

Another plausible way to protect Mg alloys from corrosion attack inside physiological environment while maintaining a good level of bioactivity are by through coating process. CaP coating has been successfully applied as bioactive coating, which not only provide corrosion protection, but also biocompatible and nontoxic [3]. Previous projects have successfully coated CaP onto the metallic implant substrates such as titanium [11] and Mg [12–18]. The application method for CaP are relatively varied from as simple as direct chemical immersion [3,12,13,15–18] and to a more advanced technique such as plasma spraying and pulse laser deposition method as been reviewed previously [1,19]. However, advance techniques which require high temperature are not a suitable way for coating CaP onto Mg because of their low melting temperature and poor heat resistance [10,17]. So, the simple chemical method seems to be the suitable way of coating Mg with CaP. Therefore, this research work was aimed to produce CaP coating via a chemical conversion method on Mg and study the surface characteristics, in-vitro corrosion resistance, and discussed the correlation between these two properties.

2. Materials and methods

2.1. Sample preparations and conversion coating process

An ingot of Mg with compositions of >99.9% purity was used as the substrate material. The samples were cut from the ingot into dimensions of $10 \times 10 \times 5$ mm. The samples were ground according to metallography procedure up to 1200 grit. Prior to coating processes, the samples were cleansed by using deionized water (DI). The coating procedure will be divided into two steps, which is phosphating and alkaline treatment process. For ease of reference, the phosphating will be referred as the primary coating process (PRI) and alkaline treatment as the secondary coating process (SEC). The PRI coating process conducted in order to coat the metal surfaces with calcium phosphates (CaP) compounds and followed by the SEC coating process to convert any CaP phases obtained after PRI coating into a more stable hydroxyapatite (HA). The PRI coating bath consists of the source of Ca^{2+}, source of PO_4^{3-}, and bath stabilizer, which is calcium nitrate tetrahydrate, $Ca(NO_3)_2{\cdot}4H_2O$, sodium phosphate, Na_3PO_4 and nitric acid, HNO_3, respectively.

The concentration of the Ca^{2+} and PO_4^{3-} that has been selected are $[Ca^{2+}]/[PO_4^{3-}] = 0.32$ M/0.19 M. The bath stabilizer, 1 M of HNO_3 is added in order to adjust the pH of the bath solutions. The pH value of 2.0 has been selected. The PRI coating process was conducted by immersing the samples for 60 min at 40 °C. Upon completion of the immersions, the coated samples were rinsed with DI water and ready for SEC coating. SEC treatment is intended to change the phase of the coated samples into more stable HA through alkaline treatment of the PRI coated samples in 1 M sodium hydroxide, NaOH at 80 °C for 60 min.

2.2. Characterization of the coated surface

The samples were observed by using Field Emission-Scanning Electron Microscope (FESEM) equipped with Energy Dispersive Spectroscopy (EDS) (MODEL: FEI NovaNano SEM 450). The phase analyses of the coated and uncoated samples were done by conducting X- Ray Diffraction (Model: Bruker D2 Phaser). The scanning range 2θ was set from 10° to 90°. The topographical features were further analyzed by using Atomic Force Microscopy (AFM).

2.3. Corrosion analysis

The corrosion analysis was performed in Simulated Body Fluid (SBF) at 36.5 ± 0.5 °C. The SBF was prepared according to Kokubo and Takadama's protocol [20]. A classic three-electrode cell was used with platinum as the counter electrode, a saturated calomel electrode (SCE, +0.242 V vs. SHE) as the reference electrode. The samples (working electrode) were having exposed area of 1 cm^2. The Tafel potentiodynamic polarizations (PDP) were conducted by employing scanning rate of 1 mV/s. Before executing Electrochemical Impedance Spectroscopy (EIS) measurements, the sample was immersed in SBF for 60 min to establish a stable open circuit potential (OCP). EIS measurements were carried out from 10^{-2} Hz to 10^4 Hz at OCP values. The perturbation signal amplitude is set as 10 mV/RMS. The impedance data were shown as Nyquist plots. The data were analyzed by using Autolab NOVA 1.11 software. The electrochemical parameters obtained were further exploited to predict the porosity of the coating. Coating porosity was calculated by using Eq. (1) [18]:

$$P = \left(\frac{R_{uc}}{R_p}\right) \times 10^{-(\Delta E_{corr}/\beta\alpha)} \times 100\% \quad (1)$$

Where;

P = porosity percentage.

R_{uc} = polarization resistance of Mg substrate or uncoated sample.

R_p = polarization resistance of coated sample.

$\Delta E_{corr} = E_{corr}$ coated sample $- E_{corr}$ substrate.

$\beta\alpha$ = anodic Tafel slope for substrate.

3. Results & discussion

3.1. *Surface features of the coatings*

Fig. 1 shows the FESEM observations and EDS data of the substrate and coated samples. As the uncoated (UC) substrate being coated inside primary coating bath, it could be observed that the PRI samples were covered with flakes with flower-like shapes (Fig. 1(c), (d)). The flakes have 200 μm sizes and uniformly distributed on the surface of the Mg substrate. The EDS data have provided information on the elemental composition of the coating. Note that the coating comprises of O, Mg, P, and Ca. Besides, the atomic percentage of Ca over P ratio [Ca/P] is 12.55/12.50 = 1.004, which proves that the coating were composed of DCPD [21]. Traces of O and Mg suggesting that the occurrence of $Mg(OH)_2$ accumulations inside the PRI coatings. Fig. 1(e) and (f) shows the SEC coated samples featuring of splintered flower-like flakes with some small chipping, originating from the dissolution of DCPD into HA. The surface looks smoother compared to the PRI coated. The EDS results show that it comprised of O, Mg, Na, P and Ca elements with Ca/P ratio of 17.6/9.64 = 1.8257, slightly higher than the ideal stoichiometry HA (1.67) [21]. From EDS, the Mg content is higher compared to PRI, which suggests that the SEC coated is thinner than PRI coated. This also could be contributed by the DCPD to HA conversion process. There are some traces of sodium, Na found on the surface of SEC coated. The Na may emerge from traces of NaOH solutions.

Phase analyses of the samples were illustrated in Fig. 2. From Fig. 2(a), the expected diffractogram of Mg substrate were revealed and in-line with the PDF 00-035-0821. The PRI samples were covered mainly with DCPD phases (PDF 01-072-0713). It could be observed by the occurrence of the major planes of DCPD such as (0 2 0), (1 2 $\bar{2}$), (0 4 0), (1 1 $\bar{1}$) at 2θ value of 11°, 21°, 24° and 29°. The Mg substrate peaks still observable from the diffractogram with lower intensity and this could be attributed to the good coverage and the thickness of the coating on top of the substrate surface. Fig. 2(c) confirmed that the HA phase were appeared on the surfaces after secondary coating process (PDF 01-074-7564). Besides, most of the DCPD phases that appear after primary coating are slightly disappear, which supports the observations of the dissolution process of DCPD into HA in Fig. 2(c). The Mg peaks reflection intensity is slightly increased compared to the diffractogram produced by the PRI coated sample. The re-emergence of the Mg peaks could be subjected to the $Mg(OH)_2$ phase, porous nature of the coating and the erosion process impart by the secondary coating treatment towards the sample [18]. The $Mg(OH)_2$ could not be detected by the diffractogram. This is

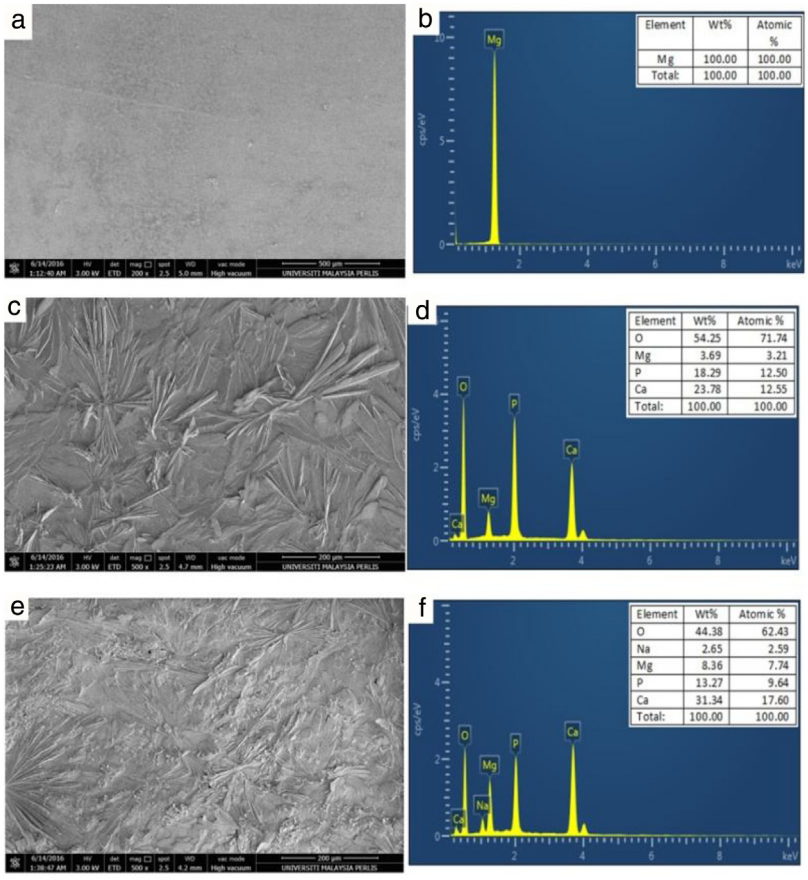

Fig. 1 – Microstructure and EDS spectra of (a,b) UC, (c,d) PRI coated, and (e,f) SEC coated samples.

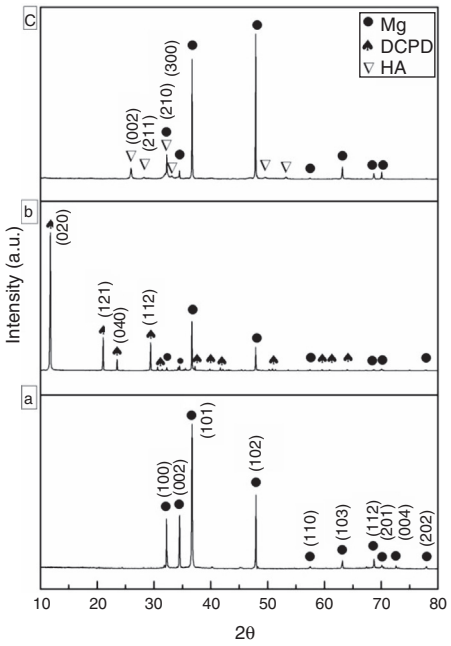

Fig. 2 – XRD spectra for (a) UC, (b) PRI coated, and (c) SEC coated samples.

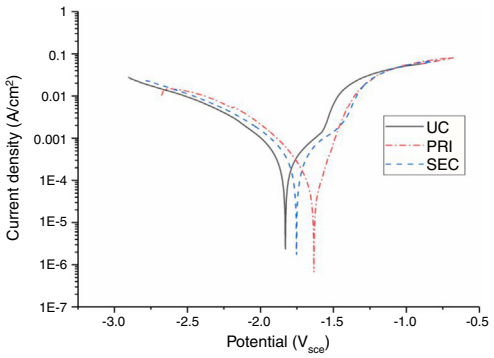

Fig. 4 – Potentiodynamic polarization curves of UC, PRI, and SEC coated samples inside SBF at 37 °C.

related to the amorphous nature of the phase and the preferred orientation of the samples.

The topographical features of the coatings were examined under AFM. The average roughness, Ra and root mean square roughness, Rq value of each sample were attached together with topographical features as depicted in Fig. 3. The AFM revealed that the UC samples composed of slightly rough uniform peaks, resulting from the grinding polishing process. The process is needed to provide texture for the interlocking between the coating and the substrate [22]. For PRI coated, the topographical features a slightly coarse shape profile with thin splinter peaks and could be linked from the flower-like flakes as evidenced in the Fig. 1(b). For SEC coated, the profile exhibit finer surface with thicker splinter compared to PRI coated. It is revealed that the PRI and SEC exhibit comparable surface roughness value. PRI sample possessed Ra and Rq values of 0.1145 μm and 0.1449 μm, while the SEC sample has slightly less rough with Ra and Rq values of 0.105 μm and 0.134 μm.

3.2. *Corrosion analysis*

PDP of the coated and uncoated samples were executed inside SBF at 37 °C and the results were illustrated in Fig. 4. The electrochemical parameter obtained from the polarization curves were tabulated in Table 1. It could be stated that the coatings improved the corrosion resistance of the samples. The E_{corr} of PRI and SEC coated samples shifts towards nobler directions compared to the UC sample. The polarization current density (i_{corr}) of the coated samples is also smaller compared to the UC. The cathodic branch of the PDP curves representing the hydrogen evolution process [15], denoted by Eq. (2);

$$2H_2O + 2e^- \rightarrow 2OH^- + H_2 \quad (2)$$

The βc of the three samples are within range of −120 mV/dec to −300 mV/dec, which confirms the water reduction process with the release of hydrogen gas such as

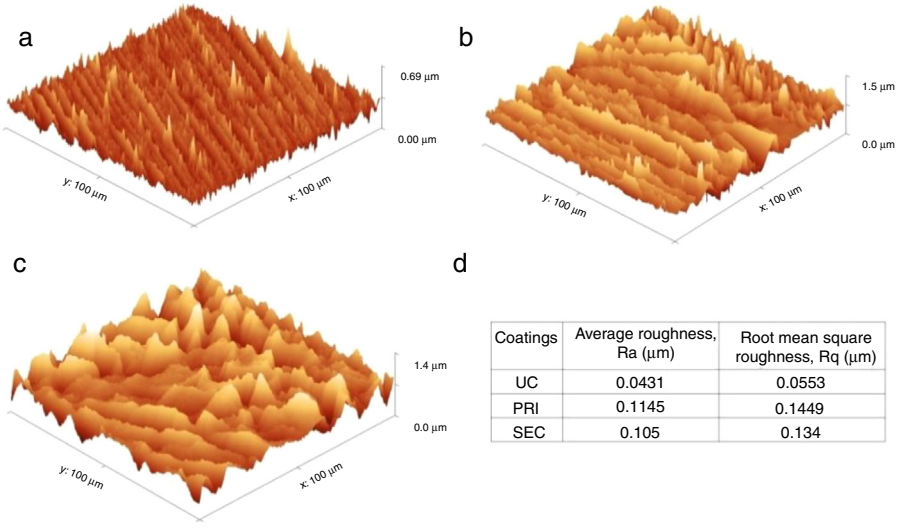

Coatings	Average roughness, Ra (μm)	Root mean square roughness, Rq (μm)
UC	0.0431	0.0553
PRI	0.1145	0.1449
SEC	0.105	0.134

Fig. 3 – Topographical features of (a) UC, (b) PRI, (c) SEC samples and (d) Ra and Rq values of each sample.

Table 1 – Electrochemical parameters from PDP of UC, PRI, and SEC samples immersed inside SBF at 37 °C.

	$B\alpha$ (mV/dec)	Bc (mV/dec)	E_{corr} (V vs. SCE)	i_{corr} (μA/cm^2)	Coating porosity (%)
UC	225.3967 ± 38	−191.057 ± 20	−1.8404 ± 0.01	185.7647 ± 16	–
PRI	81.6977 ± 6	−82.358 ± 2	−1.6286 ± 0.07	25.2552 ± 6	0.3
SEC	135.65 ± 41	−135.345 ± 412	−1.7612 ± 0.01	120.9897 ± 26	22.6

denoted by Eq. (2) [15,23]. The anodic branch of the PDP curves representing the dissolutions of the Mg substrates [15], denoted by Eq. (3);

$$Mg \rightarrow Mg^{2+} + 2e^{-} \quad (3)$$

The βα of the three samples are within range of 30 mV/dec to 320 mV/dec, in the same agreement with Eq. (3) and results from previous studies [15]. Deflection points at anodic branch of UC and SEC curves could be observed at −1.55 V and 1.45 V, respectively. The sudden increment in current density, which yield these deflections points denotes the beginning of pitting corrosion, E_{pt} [24]. The PRI sample is more corrosion resistance compared to the SEC and UC. This is the main reasons for the vague E_{pt} point for PRI. Besides, the high corrosion resistance of the PRI coated could be the results of the absence of secondary coating treatment process. The dissolution process of DCPD into HA phases through secondary coating treatment could leave some micro-pores and cracking that slightly assisted corrosion attack by providing sites for the corrosion attacks to progress. Additionally, it is suggested that the PRI coating is thicker compared to the SEC. The thinning of the SEC coating is due to the erosion resulted from the DCPD dissolutions [25]. This is supported by the prediction of coating porosity for PRI and SEC coated samples calculated by using Eq. (1). As it could be observed, the PRI produced the lowest porosity value, about 0.3% and SEC sample has porosity up to 22.6%.

Following the polarization, the samples were further examined by using EIS. The Nyquist plot of UC, PRI and SEC samples were plotted and presented in Fig. 5. All samples exhibited 2 times constant. Noted that PRI sample also has 2 time constants with both of the semicircle is overlapped. Theoretically, lower-frequency is subject to solution–substrate interface and higher-frequency time constant is subjected to solution-coating interfaces [25]. It could be observed that dimension of the semicircle is in order of PRI □ SEC □ UC. The diameter of the semicircle is directly proportional to the corrosion resistance of the samples [25,26]. Hence, it is direct evidence that the PRI sample has superior corrosion resistance performance, followed by the SEC and UC samples. The Nyquist plot is complementing the PDP results as depicted in Fig. 4.

To further understand the corrosion characteristics of the samples, EIS impedance data for UC, PRI and SEC were fitted to the equivalent electrical circuit (EEC) as depicted in Fig. 5(c). All of the fittings are less than 0.05 ($P < 0.05$), hence the EEC fittings are acceptable. According to the Nyquist plot in Fig. 5, all samples yield two loops at high frequency (HF) and medium frequency (MF). The HF loop was denoted by R_1 and CPE_1 and the MF loop denoted by R_2 and CPE_2. For coated samples, the HF is associated with the dielectric properties of the DCPD and HA coatings [16,17] and the MF is suggested to be related to the inner layer of $Mg(OH)_2$. For UC, the HF is suggested for $Mg(OH)_2$ layer and MF is for the MgO layer. Rs stand for solution resistance and CPE is the constant phase element. According to the literature, the CPE is can be further defined by two values; which is admittance (Y) and power index number (n), given by $Y = Y_0(j\omega)^n$ [16–18]. The value of n is used to represent the electrical properties of the coatings. n values vary from 1 for pure

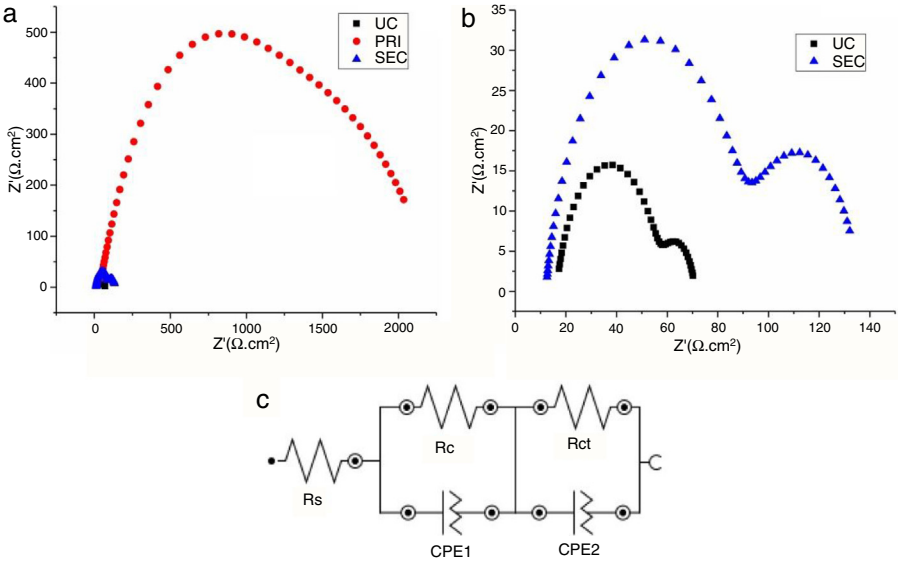

Fig. 5 – Nyquist plot for (a) all samples, (b) magnified view of UC and SEC and (c) equivalent electrical circuit of the samples in SBF.

Table 2 – EIS Fitting of the samples inside SBF solutions at 37 °C.

	Rs ($\Omega\,cm^2$)	R_1 ($\Omega\,cm^2$)	Y_1 (μMho)	n_1	R_2 ($\Omega\,cm^2$)	Y_2 (μMho)	n_2
UC	8.6 ± 1	42.15 ± 1	79.75 ± 3	0.822 ± 0.01	16.1 ± 4	$4.61 \times 10^{-3} \pm 0.0005$	0.835 ± 0.02
PRI	20.73 ± 8	1423.33 ± 185	25.33 ± 66	0.509 ± 0.014	85.67 ± 105	$5.47 \times 10^{-3} \pm 0.001$	0.794 ± 0.04
SEC	15.03 ± 0.2	70.3 ± 10	56.4 ± 4	0.838 ± 0.003	44.63 ± 5	$7.39 \times 10^{-3} \pm 0.001$	0.7547 ± 0.03

capacitive behaviour (flat surface) and 0.5 for porous surface [27]. The CPE was utilized in the proposed EEC model for better fit. Besides, Nyquist plot of all samples exhibit depressed semicircle (Fig. 5) thus, which makes the CPE is the most suitable selection for the proposed EEC model [28].

EIS fittings were tabulated in Table 2. The polarization resistance, R_p of the samples is accounted by the total resistance imparted from the R_1 and R_2 values. It should be noted that the coatings improved the corrosion resistance of the samples. The PRI and SEC coating improved the R_p of the samples almost 40 times and 2 times greater than the UC, respectively. However, it is clear that the corrosion resistance of the PRI coated is superior compared to the SEC. It is proven by the lowest value of admittance, Y_1 of the HF loop exhibited by the PRI sample. The low n_1 value, suggesting that the PRI coated is porous and rough. The Y_1 value of HF loop of the SEC is higher compared to the PRI, denoting that it is less corrosion resistant than PRI. As discussed by Su et al., they stated that the value of admittance, Y is given by $Y \approx \varepsilon\varepsilon_0 A/d$, where; ε is the dielectric constant of coating, ε_0 is the dielectric constant of free space, A is the exposed coating area and d is the coating thickness [25]. From the equations, it could be stated that the Y_1 value is inversely proportional to the coating thickness, d. Hence, the increment of Y_1 value of SEC confirmed that the alkaline treatment lowering the corrosion resistance of the samples by lowering the coating thickness. The n_1 value for the SEC is higher, suggesting that due to the secondary alkaline treatment, the SEC coat becomes denser and the coatings become less rough. Moving towards the MF loops, the R_2 values produced by all of the samples are lower compared to the R_1 values. This shows that the $Mg(OH)_2$ and MgO layers also imparts some degree of resistance towards corrosion attacks, even though the value is far more less compared to the PRI and SEC coatings. The Y_2 and n_2 values are comparable for each sample.

The coatings of DCPD and HA protects the samples by minimizing the contact area between the surrounding solutions and the substrate surface. As discussed, the DCPD coat on the PRI sample have better coating coverage throughout the sample surface and low porosity that helps minimize the ionics penetration of corrosion attack from adjacent solutions. Conversely, SEC with HA coatings possessed higher porosity and lower thickness. Besides, surface roughness of PRI is comparable to SEC coated, which means both coatings have an equivalent exposed area to the corrosion media. From the biomaterials point of views, HA phase is more favoured because of its bioactivity and similarity with bone minerals. Besides, HA is more stable compared to DCPD [29]. It is suggested that tailoring the deposition coating time could further improve the properties of the coatings. As an example, the primary treatment time could be prolonged in order to produce a thicker DCPD coating on the substrate. Then, the secondary treatment time could be shortened or extend accordingly. Then the conversion of DCPD into HA by secondary treatment could be done and minimizing the dissolution and erosion of the treatment. It is suggested in the future that the effect of both coating time on the corrosion performance of Mg is conducted in order to extend our knowledge.

4. Conclusion

CaP coating on the pure Mg substrate was successfully produced by using a simple chemical conversion method. The surface features characterization of both PRI and SEC coated samples revealed that the coatings exhibit the flower like shape features. The phase analysis confirms the formation of DCPD phase for PRI sample and HA phase for SEC samples. The electrochemical corrosion analysis revealed that both coatings have improved the corrosion resistance of pure Mg inside SBF. It is revealed that the PRI possessed higher corrosion resistance compared to the SEC. It is confirmed that the alkaline treatment has made the SEC more prone to corrosion. This is because the treatment has imparted erosion to the samples which will lead to thinning of the coating and porosity. However, the secondary coating treatment is needed in order to convert the DCPD to a stable HA. The processing parameters are suggested to be the decisive factors on the performance of the HA coated Mg. Nevertheless, future work should focus on systematic studies or optimization of primary and secondary coating parameters on properties of final coated products.

Conflicts of interest

The author declares that there is no conflict of interest.

Acknowledgements

The authors are grateful for the financial support from the Fundamental Research Grant Scheme (FRGS) [FRGS/1/2015/SG06/UNIMAP/01/1] from the Ministry of Higher Education Malaysia (MoHE) and Universiti Malaysia Perlis (UniMAP) for the facilities provided.

REFERENCES

[1] Shadanbaz S, Dias GJ. Calcium phosphate coatings on magnesium alloys for biomedical applications: a review. Acta Biomater 2012;8:20–30.
[2] Staiger MP, Pietak AM, Huadmai J, Dias G. Magnesium and its alloys as orthopedic biomaterials: a review. Biomaterials 2006;27:1728–34.

[3] Brundavanam S, Eddy G, Poinern J, Fawcett D. Growth of flower-like brushite structures on magnesium substrates and their subsequent low temperature transformation to hydroxyapatite. Am J Biomed Eng 2014;4:79–87.
[4] Eddy G, Poinern J, Brundavanam S, Fawcett D. Biomedical magnesium alloys: a review of material properties surface modifications and potential as a biodegradable orthopaedic implant. Am J Biomed Eng 2012;2:218–40.
[5] liang CHENGY, wei QINT, min WANGH, Zhang Z. Comparison of corrosion behaviors of AZ31, AZ91 AM60 and ZK60 magnesium alloys. Trans Nonferrous Met Soc China (English Ed) 2009;19:517–24.
[6] Hort N, Huang Y, Fechner D, Störmer M, Blawert C, Witte F, et al. Magnesium alloys as implant materials – principles of property design for Mg-RE alloys. Acta Biomater 2010;6:1714–25.
[7] González S, Pellicer E, Fornell J, Blanquer A, Barrios L, Ibáñez E, et al. Improved mechanical performance and delayed corrosion phenomena in biodegradable Mg–Zn–Ca alloys through Pd-alloying. J Mech Behav Biomed Mater 2012;6:53–62.
[8] Li N, Zheng Y. Novel magnesium alloys developed for biomedical application: a review. J Mater Sci Technol 2013;29:489–502.
[9] Zaludin MAF, Jamaludin SB, Idris MS, Llah NA. Effect of 45S5 bio-glass particles on physical properties and corrosion resistance of the Mg–5Zn matrix composite. Chem Mater Sci 2014:1–8.
[10] Razavi M, Fathi MH, Meratian M. Microstructure, mechanical properties and bio-corrosion evaluation of biodegradable AZ91-FA nanocomposites for biomedical applications. Mater Sci Eng A 2010;527:6938–44.
[11] Ohtsu N, Nakamura Y, Semboshi S. Thin hydroxyapatite coating on titanium fabricated by chemical coating process using calcium phosphate slurry. Surf Coatings Technol 2012;206:2616–21.
[12] Xu L, Pan F, Yu G, Yang L, Zhang E, Yang K. In vitro and in vivo evaluation of the surface bioactivity of a calcium phosphate coated magnesium alloy. Biomaterials 2009;30:1512–23.
[13] Chen XB, Birbilis N, Abbott TB. A simple route towards a hydroxyapatite–$Mg(OH)_2$ conversion coating for magnesium. Corros Sci 2011;53:2263–8.
[14] Wang H, Guan S, Wang Y, Liu H, Wang H, Wang L, et al. In vivo degradation behavior of Ca-deficient hydroxyapatite coated Mg–Zn–Ca alloy for bone implant application. Colloids Surfaces B Biointerfaces 2011;88:254–9.
[15] Su Y, Li G, Lian J. A chemical conversion hydroxyapatite coating on AZ60 magnesium alloy and its electrochemical corrosion behaviour. Int J Electrochem Sci 2012;7(11):497–511.
[16] Su Y, Lu Y, Su Y, Hu J, Lian J, Li G. Enhancing the corrosion resistance and surface bioactivity of a calcium-phosphate coating on a biodegradable AZ60 magnesium alloy via a simple fluorine post-treatment method. RSC Adv 2015;5:56001–10.
[17] Su Y, Li D, Su Y, Lu C, Niu L, Lian J, et al. Improvement of the biodegradation property and biomineralization ability of magnesium–hydroxyapatite composites with dicalcium phosphate dihydrate and hydroxyapatite coatings. ACS Biomater Sci Eng 2016;2:818–28.
[18] Su Y, Guo Y, Huang Z, Zhang Z, Li G, Lian J, et al. Preparation and corrosion behaviors of calcium phosphate conversion coating on magnesium alloy. Surf Coatings Technol 2016;307:99–108.
[19] Surmenev RA, Surmeneva MA, Ivanova AA. Significance of calcium phosphate coatings for the enhancement of new bone osteogenesis – a review. Acta Biomater 2014;10:557–79.
[20] Kokubo T, Takadama H. How useful is SBF in predicting in vivo bone bioactivity? Biomaterials 2006;27:2907–15.
[21] Dorozhkin SV. Calcium orthophosphate coatings, films and layers. Prog Biomater 2012;1:1.
[22] Dunne CF, Twomey B, O'Neill L, Stanton KT. Co-blasting of titanium surfaces with an abrasive and hydroxyapatite to produce bioactive coatings: substrate and coating characterisation. J Biomater Appl 2014;28:767–78.
[23] Baril G, Galicia G, Deslouis C, Pébère N, Tribollet B, Vivier V. An impedance investigation of the mechanism of pure magnesium corrosion in sodium sulfate solutions. J Electrochem Soc 2007;154:C108–13.
[24] Srinivasan A, Shin KS, Rajendran N. Dynamic electrochemical impedance spectroscopy (DEIS) studies of AZ31 magnesium alloy in simulated body fluid solution. RSC Adv 2014;4:27791–5.
[25] Su Y, Niu L, Lu Y, Lian J, Li G. Preparation and corrosion behavior of calcium phosphate and hydroxyapatite conversion coatings on AM60 magnesium alloy. J Electrochem Soc 2013;160:C536–41.
[26] Wang B, Huang P, Ou C, Li K, Yan B, Lu W. In vitro corrosion and cytocompatibility of ZK60 magnesium alloy coated with hydroxyapatite by a simple chemical conversion process for orthopedic applications. Int J Mol Sci 2013;14:23614–28.
[27] El-Taib Heakal F, Shehata OS, Tantawy NS. Degradation behaviour of AZ80E magnesium alloy exposed to phosphate buffer saline medium. Corros Sci 2014;86:285–94.
[28] Jamesh M, Kumar S, Sankara Narayanan TSN. Corrosion behavior of commercially pure Mg and ZM21 Mg alloy in Ringer's solution – long term evaluation by EIS. Corros Sci 2011;53:645–54.
[29] Morteza S, Shahri G, Assadian M, Hasbullah M. Hydroxyapatite and fluoridated hydroxyapatite coatings and their effects on commercially pure magnesium corrosion response. Trans Indian Inst Met 2016.